Support information for

Isotopic signatures of methane emission from oil and natural gas plants in southwestern China

Dingxi Chen[1†], Yi Liu[2†], Zetong Niu[1], Ao Wang[1], Pius Otwil[1], Yuanyuan Huang[1], Zhongcong Sun[1], Xiaobing Pang[3], Liyang Zhan[4], Longfei Yu[1*]

[1]Shenzhen Key Laboratory of Ecological Remediation and Carbon Sequestration, Institute of Environment and Ecology, Tsinghua Shenzhen International Graduate School, Tsinghua University, Shenzhen 518055, China

[2]Safety, Environment and Technology Supervision Research Institute of PetroChina Southwest Oil and Gas Field Company, Chengdu 610041, China

[3]College of Environment, Zhejiang University of Technology, Hangzhou, 310014, China

[4]key Laboratory of Global Change and Marine-Atmospheric Chemistry, Third Institute of Oceanography, Ministry of Natural Resources, Xiamen, 361005, China

[*]Corresponding authors: longfei.yu@sz.tsinghua.edu.cn

[†]These authors contributed equally.

Manuscript Type: Research Article

Contents

1 Source partitioning with end-member mixing method

In this study, we used CH_4 isotopes and mixing ratios as tracers. The contribution of atmospheric background, open surface area, and facility area to the CH_4 content of the air was calculated using the following formula:

$$\delta^{13}C_m = a \cdot \delta^{13}C_1 + b \cdot \delta^{13}C_2 + c \cdot \delta^{13}C_3 \quad (1)$$

$$C_m = a \cdot C_1 + b \cdot C_2 + c \cdot C_3 \quad (2)$$

$$1 = a + b + c \quad (3)$$

Where $\delta^{13}C_m$, $\delta^{13}C_1$, $\delta^{13}C_2$, $\delta^{13}C_3$ represent CH_4 isotopes in the air, the atmospheric background, the surface open area and the facility area, respectively; and a, b, c represent the contributions of the atmospheric background, the surface open area and the facility area, respectively; C_m, C_1, C_2, C_3 represent CH_4 mixing ratios in the air, the atmospheric background, the surface open area, and the facility area, respectively (results were shown in SI, Table S4). The values of a, b, and c can be obtained by combining equation (1), (2), (3).

2 Sensitivity analysis with the updated source isotope signatures of CH_4 from the Chinese ONG industry

As the isotopic signatures of major anthropogenic CH_4 sources may act as important benchmarks for estimating global emission budgets[1], we applied a back-of-the-envelope calculation based on the revised isotope signatures for the Chinese ONG industry from our study. The computation processes are indicated as below:

$$Q_T = Q_{FF} + Q_{mic} + Q_{BB} \quad (4)$$

Where Q_T, Q_{FF}, Q_{mic}, and Q_{BB} represent the total CH_4 emission of global, fossil fuel, microbial, and biomass burning sources, respectively.

$$Q_T \cdot \delta^{13}C_Q = Q_{FF} \cdot \delta^{13}C_{FF} + Q_{mic} \cdot \delta^{13}C_{mic} + Q_{BB} \cdot \delta^{13}C_{BB} \quad (5)$$

Where $\delta^{13}C_Q$ is the combined signal of $\delta^{13}C$ emitted to the atmosphere. $\delta^{13}C_{FF}$, $\delta^{13}C_{mic}$, and $\delta^{13}C_{BB}$ represent the $\delta^{13}C$ of global fossil fuel, microbial, and biomass burning sources, respectively.

The abundance of CH_4 isotopes ($\delta^{13}C$) in the atmosphere is determined by the global sources of CH_4 and their contribution ratios, including fossil fuels (oil and natural gas, coal), biomass burning and microbial sources (wetland, ruminant, termites, rice and landfill/waste, etc.). Each source has different isotope signal values ($\delta^{13}C$); details are show in SI, Table S5, and these data were obtained from the global CH_4 isotope database[1]. The global ground-based CH_4 and $\delta^{13}C$ data (monthly average data) are available from the NOAA server (https://gml.noaa.gov/dv/data/), and results are shown in SI, Fig. S8. At the same time, global CH_4 emissions data are available from Saunois, M. et al.[2].

In order to calculate the effect of this study's results on the global flux of fossil fuel, and microbial sources, we based on the following assumptions: (1) since CH_4 emissions from biomass sources are relatively small (less than 10%), the contribution ratio is constant; (2) $\delta^{13}C_{mic}$ and $\delta^{13}C_{BB}$ are also constant which from recent research; (3) the results of this study represent the $\delta^{13}C$-CH_4 (-21.95‰, the average of 11 stations) signature of the region from ONG, and we modified $\delta^{13}C_{FF}$ based on our results and weighted (Eq. (6)). Because of the timeliness of the data, we calculated the Q_{FF} and Q_{mic} for the 2010-2019 decades with equation (4) and (5).

$$\delta^{13}C_{FF} = f_1 \cdot \delta^{13}C_1 + f_2 \cdot \delta^{13}C_{FFG} \quad (6)$$

Where f_1 represents the ratio of CH_4 emissions from China's ONG sector to global CH_4 emissions from fossil fuel, and f_2=1-f_1. $\delta^{13}C_{FFG}$ (-44‰) represents the average $\delta^{13}C$ of global fossil fuel, and $\delta^{13}C_1$ (-21.95‰) represents the average $\delta^{13}C$ of Chinese ONG sector based on this study.

The detailed calculations are shown below:

The global CH_4 emissions data from Saunois, M. et al.[2], for 2010-2019 decades, the total emission (excluding other natural sources) was 571 Tg CH_4 yr^{-1}, the fossil fuel sources ,the biomass and burning sources and the microbial sources emission was 117.5 Tg CH_4 yr^{-1}, 27.5 Tg CH_4 yr^{-1}, and 426 Tg CH_4 yr^{-1}, respectively. So, the global contribution of fossil fuel sources, biomass and burning sources and microbial sources was 20.58%, 4.81% and 74.61%, respectively. In addition, CH_4 emissions from China's ONG industry account for approximately 2.5% of global CH_4 emissions from fossil sources[3]. The $\delta^{13}C$ signatures of each CH_4 source from SI, Table S5.

According equation (5), (6) and relevant data above:

$\delta^{13}C_Q$= 20.58%×(-44‰) + 4.81%×(-22.2‰) + 74.61%×(-62.2‰) = -56.53‰;

and $\delta^{13}C_{FF}$=2.5%× (-44‰) + 97.5%× (-44‰) =-43.45‰;

Then, based on the relevant assumptions and equation (4) and (5), where $\delta^{13}C_Q$ = -56.53‰, $\delta^{13}C_{FF}$=-43.45‰.

From the calculations, we found that Q_{FF}=19.97%, indicated that the CH_4 emissions from fossil fuel sources was overestimated by 0.61%, this corresponds to an overestimation of emissions by 3.47 Tg CH_4 yr^{-1}. Microbial sources were underestimated to the same extent.

Table S1 $\delta^{13}C$ in part large ONG basins of China

Basin	Area	Production layer	$\delta^{13}C_{CH4}$ (‰)	Reference
Tarim Basin	Platform area of Tarim Basin	O	-42.6~ -32	[4]
Sichuan Basin	Sichuan Basin	C, P, T	-37~ -27	
Ordos Basin	Lower Paleozoic of Ordos Basin	O	-40.3~ -31	
Liaohe Basin	Western part of Liaohe Depression	E	-54.8~ -31	[5]
Huanghua Depression	Huanghua Depression	E	-47.3~ -36.8	[6]
Tarim Basin	Platform area of Tarim Basin	∈, O	-45.4~ -32.0	
Sichuan Basin	Northeastern Sichuan Basin	S	-32.5~ -27.0	
Songliao Basin	Songliao	J-K	-32.7~ -17.4	[7]
Sichuan Basin	Wolonghe Field	T, P, C	-34.5~ -31.69	[8]
Sichuan Basin	Weiyuan Field	Z	-32.38~ -32.37	
Sichuan Basin	East Sichuan Basin	P, T	-34.5~ -28.9	
Sichuan Basin	East Sichuan Basin	T	-32.35~ -29.52	[9]
Sichuan Basin	Northeastern Sichuan Basin	P, T	-37.44~ -29.4	[10]
Zhujiangkou	Panyu30-1	N	-33.89	[11]
Tarim Basin	Tazhong Uplift	O	-54.9~ -35.7	[12]
Sichuan Basin	Sichuan Basin	Z, ∈, C, P, T	-37.9~ -28.5	[13]

Table S2 The information of samples from oil and natural gas production sites

Site	Site No.	Sampling location	Time	No.	Average $\delta^{13}C$ (‰)	Average CH_4 (ppm)
MX	S1	Pipeline area	4.13	MX-01	-47.24	2.03
		H: 100 m	4.13	MX-02	-47.92	1.99
		H: 50 m	4.13	MX-03	-47.58	1.97
		H: 100 m	4.13	MX-04	-46.88	1.99
		H: 50 m	4.13	MX-05	-46.84	1.98
		Production area	4.13	MX-06	-47.82	2.01
		Ground	4.13	MX-07	-42.27	2.40
		Production area	4.13	MX-08	-46.42	2.05
SN	S2	H: 200 m	4.14	SN-01	-46.49	1.98
		H: 300 m	4.14	SN-02	-47.13	1.88
		H: 100 m	4.14	SN-03	-48.30	1.97
		Production area	4.14	SN-04	-31.61	3.49
		Production area	4.14	SN-05	-44.92	2.07
		H: 50 m	4.14	SN-06	-45.66	2.02
		H: 200 m	4.14	SN-08	-47.19	2.00
		Ground	4.14	SN-09	-47.07	2.05
		H: 50 m	4.14	SN-11	-46.97	1.97
		Pipeline area	4.14	SN-12	-30.97	3.66
		Pipeline area	4.14	SN-13	-44.49	2.22
XBQ	S3	Ground	4.15	HJB-01	-45.51	2.17
		Pipeline area	4.15	HJB-02	-47.98	2.01
		H: 300 m	4.15	HJB-03	-47.02	1.97
		H: 200 m	4.15	HJB-04	-47.28	2.06
		H: 100 m	4.15	HJB-05	-48.11	1.91
		H: 50 m	4.15	HJB-06	-47.36	1.99
XQ	S4	Ground	4.15	SZG-01	-45.10	2.15
		Pipeline area	4.15	SZG-02	-38.79	2.61
		Well	4.15	SZG-03	-45.76	2.14
		H: 300 m	4.15	SZG-04	-47.27	1.96
		H: 200 m	4.15	SZG-05	-45.97	1.88
		H: 100 m	4.15	SZG-06	-45.80	2.03
		H: 50 m	4.15	SZG-07	-45.69	1.91
DQ	S5	Ground	4.16	NMG-01	-46.97	2.00
		Pipeline area	4.16	NMG-02	-44.58	1.99
		H: 300 m	4.16	NMG-03	-47.03	1.98
		H: 200 m	4.16	NMG-04	-46.76	1.98
		H: 100 m	4.16	NMG-05	-47.31	1.98
		H: 50 m	4.16	NMG-06	-46.47	1.95
XM	S6	Ground	4.16	XM-01	-46.44	1.98

Table S2 continued

		Pipeline area	4.16	XM-02	-47.15	1.99
		H: 300 m	4.16	XM-03	-45.72	2.14
		H: 200 m	4.16	XM-04	-45.86	2.14
		H: 100 m	4.16	XM-05	-48.45	1.98
		H: 50 m	4.16	XM-06	-47.14	2.01
QTCSN	S7	Ground	4.17	QTC-01	-44.19	2.24
		Pipeline area	4.17	QTC-02	-38.41	2.95
		H: 300 m	4.17	QTC-03	-45.37	2.05
		H: 200 m	4.17	QTC-04	-47.23	2.00
		H: 100 m	4.17	QTC-05	-45.86	2.15
		H: 50 m	4.17	QTC-06	-47.60	2.00
QTCSZ	S8	Ground	4.17	QTCSZ-01	-45.92	2.15
		Pipeline area	4.17	QTCSZ-02	-39.81	2.45
		H: 300 m	4.17	QTCSZ-03	-45.13	2.05
		H: 200 m	4.17	QTCSZ-04	-46.18	2.14
		H: 100 m	4.17	QTCSZ-05	-45.45	2.14
		H: 50 m	4.17	QTCSZ-06	-44.55	2.09
LHZ	S9	Ground	4.18	LHZ-01	-45.09	2.17
		Pipeline area	4.18	LHZ-02	-45.43	2.17
		H: 300 m	4.18	LHZ-03	-47.16	1.98
		H: 200 m	4.18	LHZ-04	-44.28	2.13
		H: 100 m	4.18	LHZ-05	-45.90	2.02
		H: 50 m	4.18	LHZ-06	-47.89	1.99
L1	S10	Ground	4.18	L1-01	-43.52	2.06
		Pipeline area	4.18	L1-02	-45.06	2.19
		H: 300 m	4.18	L1-03	-44.75	2.15
		H: 200 m	4.18	L1-04	-44.47	2.04
		H: 100 m	4.18	L1-05	-46.26	2.13
		H: 50 m	4.18	L1-06	-45.06	2.02
ZYZ	S11	Ground	4.19	ZHZ-01	-47.63	1.98
		Pipeline area	4.19	ZHZ-02	-44.94	2.10
		H: 300 m	4.19	ZHZ-03	-45.36	2.00
		H: 200 m	4.19	ZHZ-04	-45.72	2.04
		H: 100 m	4.19	ZHZ-05	-46.58	1.99
		H: 50 m	4.19	ZHZ-06	-44.57	2.13
Well		Leak	4.11	YJ-01	-15.40	118.98
		Leak	4.11	YJ-02	-24.01	47.00
		Ground	4.11	YJ-03	-40.30	2.79
Urban		Park	4.12	GY-01	-45.68	2.15
		Park	4.12	GY-02	-46.49	2.03
		Riverside	4.12	GY-03	-46.55	1.99
		Riverside	4.12	GY-04	-47.05	1.99

Table S3 The results of HYSPLIT model and meteorological station at sites

sites	Ground		H: 50 m		H: 100 m		H: 200 m		H: 300 m	
	Wind speed (m/s)	Wind direction	Wind speed (m/s)	Wind direction	Wind speed (m/s)	Wind direction	Wind speed (m/s)	Wind direction	Wind speed (m/s)	Wind direction
S1	2.85/1.4	33.5°/155°	4.11	32°	3.54	32.9°	4.28	32.9°	4.00	38.2°
S2	1.69/1.63	265.7°/169°	1.75	265.2°	1.82	265.0°	1.88	264.6°	1.34	263.3°
S3	2.21/0.95	70.4°/180°	2.39	71.9°	2.60	74.8°	2.83	76.9°	3.08	86.0°
S4	2.67/1.36	164.9°/183°	3.28	165.8°	2.76	167.5°	3.65	168.5°	2.86	170.8°
S5	2.21/0.89	70.4°/157°	2.39	71.9°	2.60	74.8°	2.83	76.9°	3.08	86.0°
S6	2.67/1.38	113.1°/160°	2.73	113.9°	2.76	115.8°	2.89	116.5°	2.86	117.5°
S7	0.89/0.73	73.8°/118°	1.06	75°	1.18	94.5°	1.58	100.5°	1.93	125.2°
S8	1.98/0.96	67°/207°	1.97	68°	2.03	67.6°	2.12	67°	1.93	70.4°
S9	1.69/1	265.7°/213°	1.75	265.2°	1.82	265.0°	1.88	264.6°	1.34	263.3°
S10	1.33/1.1	259.2°/194°	1.46	261.3°	1.50	264.0°	1.74	267.5°	1.68	270.9°
S11	1.81/0.71	145.0°/228°	1.91	144.1°	2.05	143.2°	2.29	144.4°	2.39	142.2°

The table above shows data from the HYSPLIT model and meteorological stations. There were models and measurements data on the ground and only simulations at high altitudes. “XX/XX” stands for “output of HYSPLIT model/measured of metrological station” values on the ground. The measured values are expressed as mean values, and the two results were compared and analyzed (SI, Fig. 6), still has some correlation, although the surface meteorological conditions are complex and changeable. This means that HYSPLIT's simulation results are reliable.

Table S4 The results of source partitioning at sites

Site	Heights	Atmospheric background (%)	Ground (%)	Facility area (%)
S1	50 m	50	0	50
	100 m	45	0	55
S2	50 m	94	0	6
	100 m	/	/	/
	200 m	37	63	0
	300 m	100	0	0
S3	50 m	35	11	54
	100 m	/	/	/
	200 m	0	30	70
	300 m	59	15	26
S4	50 m	94	0	6
	100 m	62	30	8
	200 m	96	0	4
	300 m	85	15	0
S5	50 m	48	31	21
	100 m	34	66	0
	200 m	19	72	9
	300 m	14	86	0
S6	50 m	100	0	0
	100 m	/	/	/
	200 m	/	/	/
	300 m	/	/	/
S7	50 m	/	/	/
	100 m	80	0	20
	200 m	/	/	/
	300 m	85	0	15
S8	50 m	65	1	34
	100 m	17	73	10
	200 m	70	0	30
	300 m	71	4	25
S9	50 m	/	/	/
	100 m	53	47	0
	200 m	/	/	/
	300 m	/	/	/
S10	50 m	38	47	15
	100 m	18	0	82
	200 m	27	0	73
	300 m	32	36	32
S11	50 m	/	/	/

Table S4 continued

100 m	34	35	31
200 m	23	11	66
300 m	40	0	60

"/" represents the $\delta^{13}C$ of target value (air) which is higher or lower than the source value (atmospheric background, open surface area and facility area), and it cannot be calculated, only qualitative analysis can be performed.

Table S5 $\delta^{13}C$ signatures of each CH_4 source[1]

sources	Mean of $\delta^{13}C$ (‰)
Fossil fuel	-44
Microbial	-62.2
Biomass burning	-22.2

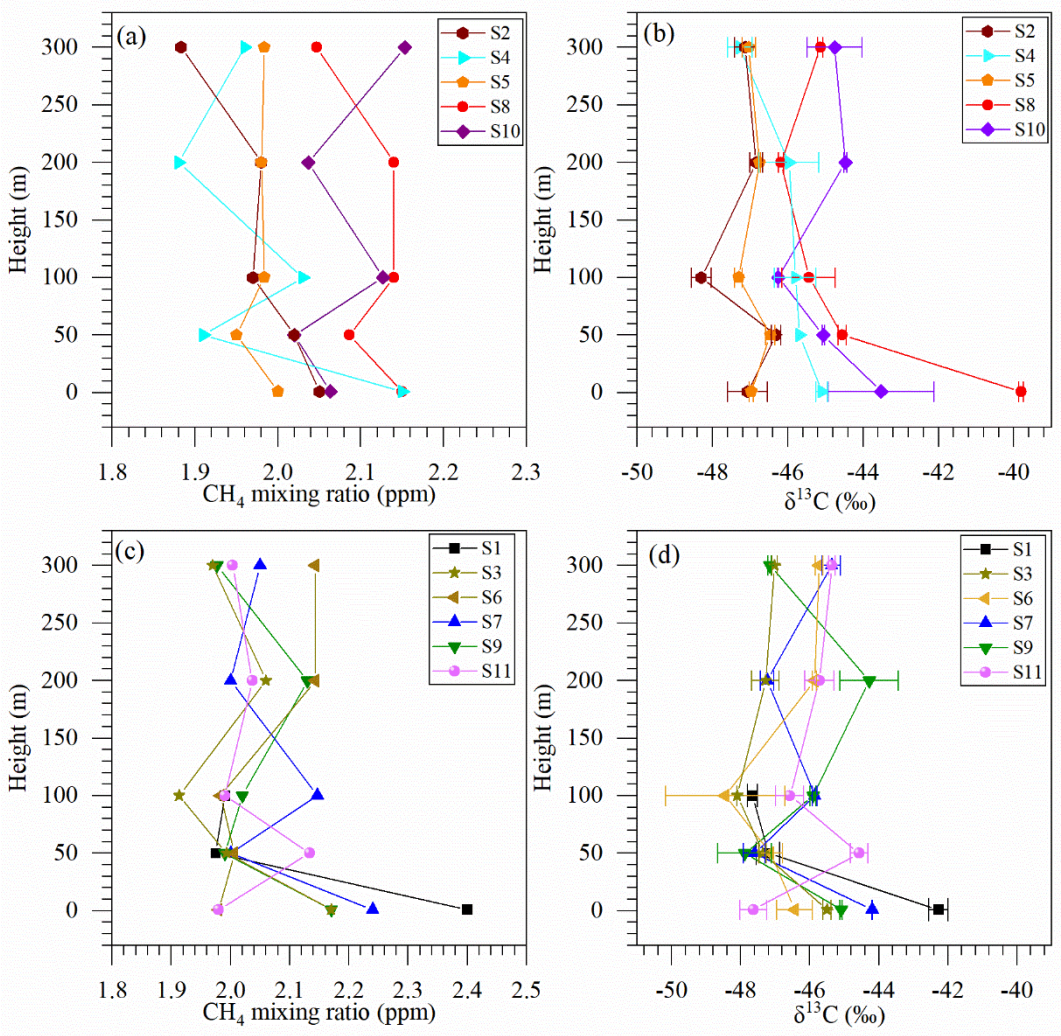

Fig. S1 Vertical variation characteristics of CH_4 mixing ratios (a, c) and isotopes (b, d) at different field stations; because of the sampling accident, only 50 m and 100 m altitude data are obtained from S1 field station, and the other stations obtained full altitude data. The variation trend of CH_4 mixing ratio and isotope vertical profile of S1, S3, S6, S7, S9, S11 and S2, S4, S5, S8, S10 sites were shown in the picture (c, d) and (a, b), respectively.

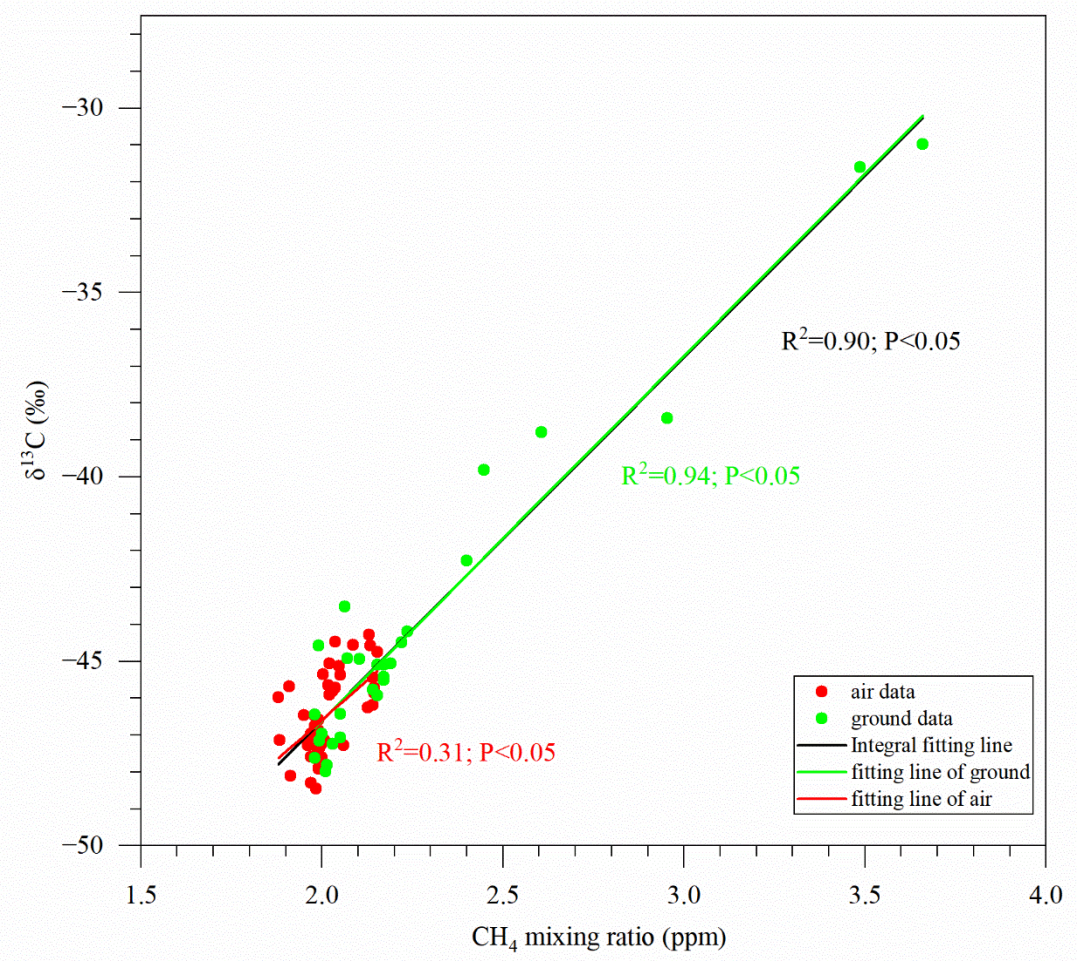

161

162 **Fig. S2** Linear fit of CH_4 mixing ratios to isotopes, data from 11 sites CH_4 samples.
163 Green and red points represent air data and ground data, respectively; black, green and
164 red lines represent integral fitting line, fitting line of ground and air, respectively; R^2
165 values are 0.90 (a), 0.94 (b), and 0.32 (c), $P<0.05$, respectively. The slopes of the black
166 and green line are very close, almost coinciding.

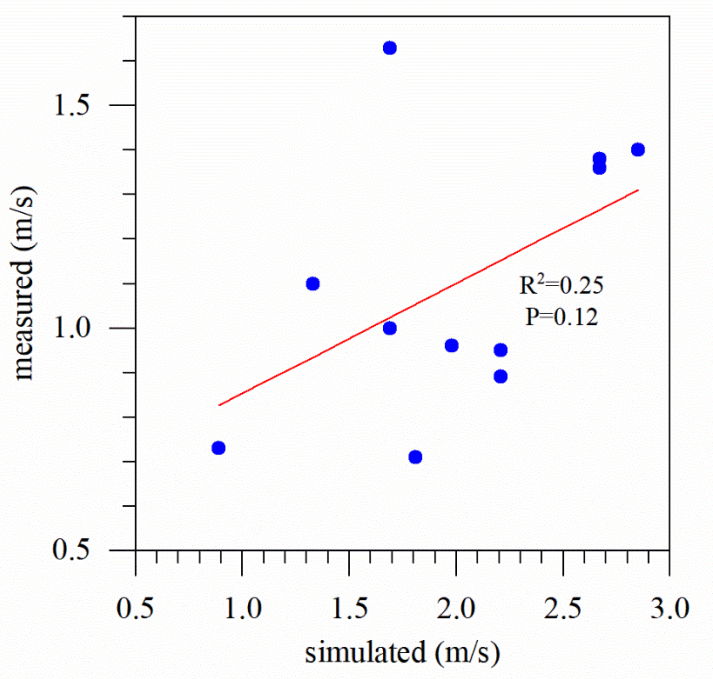

Fig. S3 The fitting analysis of the wind speed based on the HYSPLIT model and meteorological station.

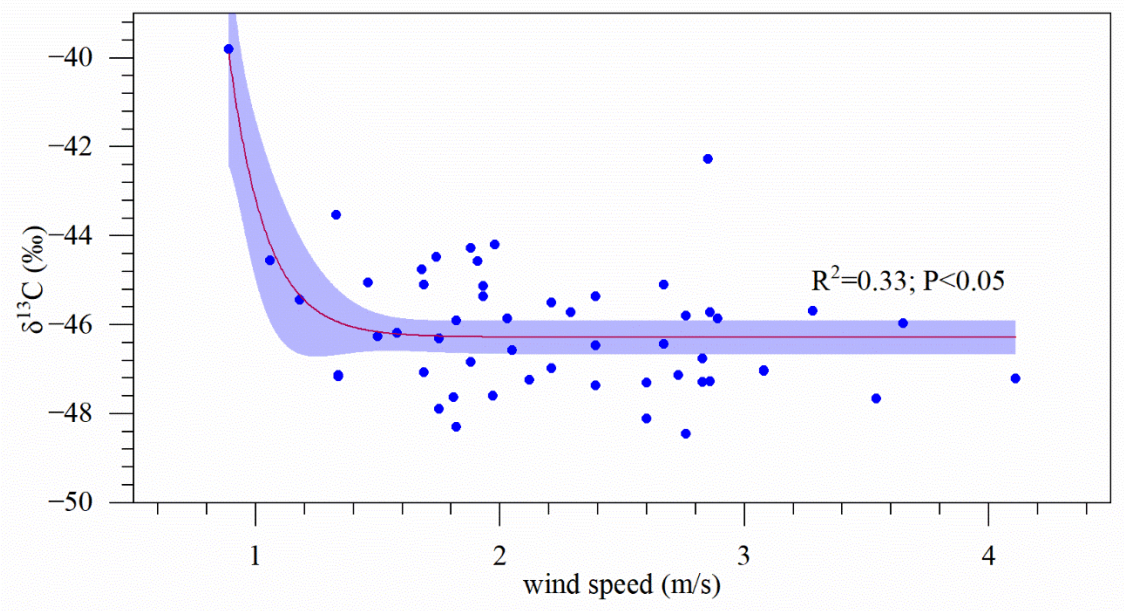

Fig. S4 Exponential correlation between wind speed and isotopes of site, wind speed and isotope data at different altitudes are included, and R^2 is 0.33, $P<0.05$. The blue area represents the 95% confidence interval and red lines represent fitting line.

Meteorological conditions, particularly wind direction, exert a significant influence on the distribution of CH_4 at the stations. The application of the HYSPLIT model is essential for understanding this phenomenon. The following example illustrates the impact of wind direction on CH_4 distribution at S7 station. During the investigation, a leak source was identified in the northeast direction of the facility area (CH_4 mixing ratios from 2.3 ppm to 13 ppm during the monitoring period). Given that the wind direction in the area where the S7 station is located was northeast, a significant increase in CH_4 mixing ratio was observed in the southwest direction of the facility area.

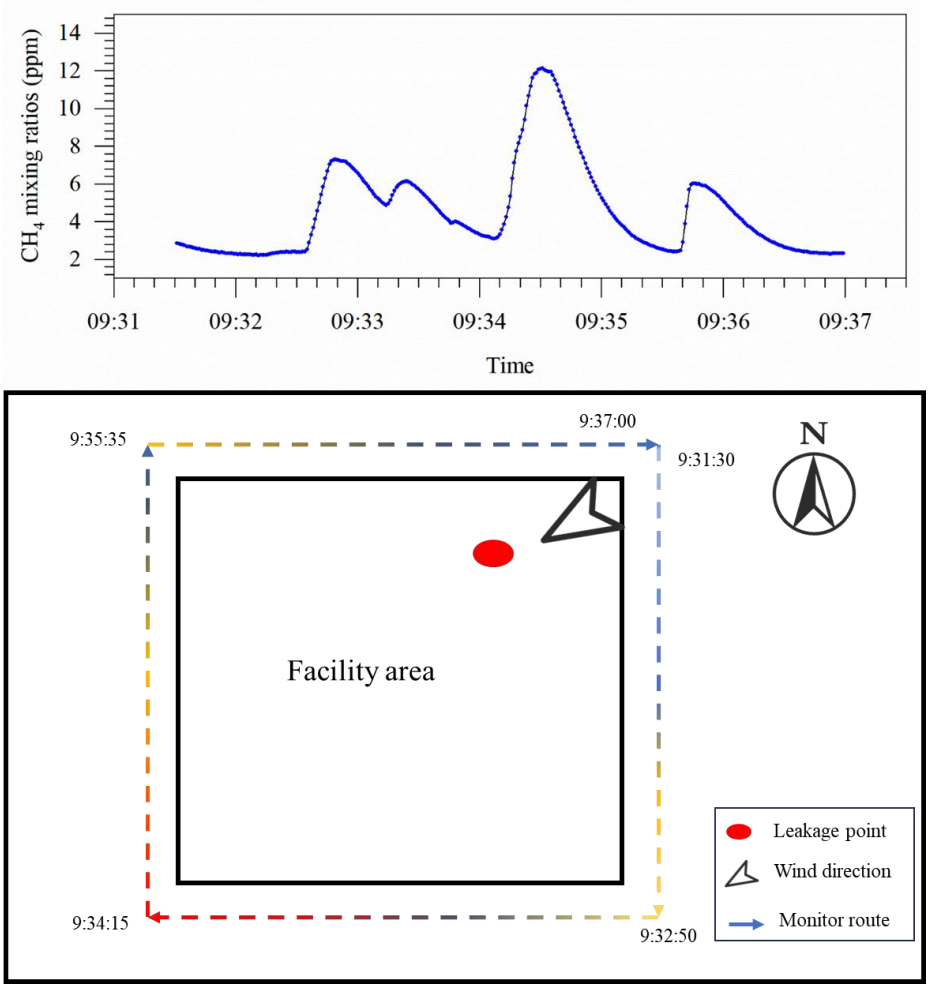

Fig. S5 Impact of meteorological conditions on the distribution of CH_4 at station S7. The upper figure shows a time-mixing ratios relationship for monitoring, while the lower figure illustrates a schematic of site monitor (schematic provided for confidentiality reasons). The dashed line indicates the monitor route, with colors representing CH_4 mixing ratios: blue for low (2~3 ppm), orange for medium (3~7 ppm), and red for high (7~12 ppm).

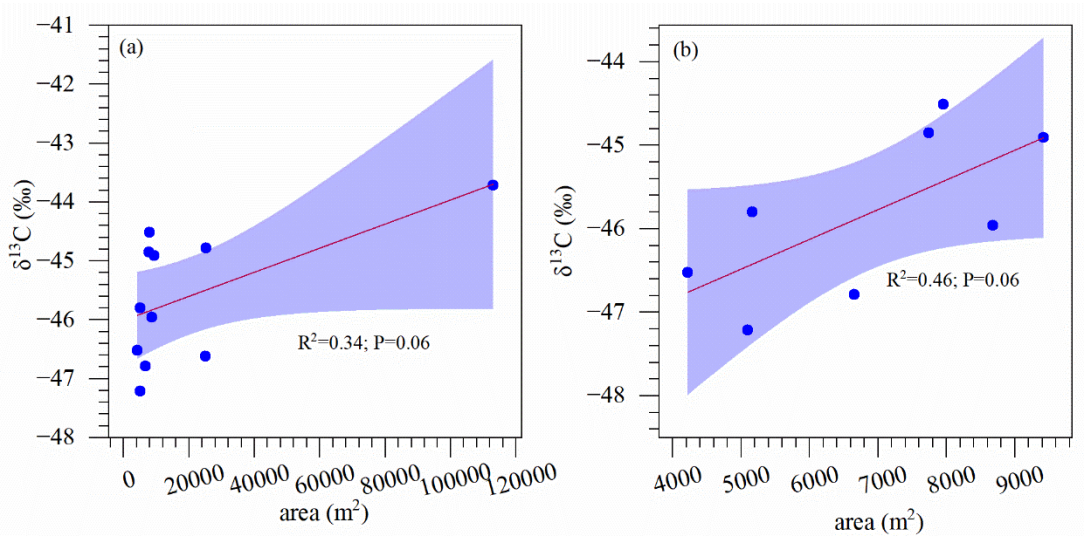

Fig. S6 Correlation between size and isotopes of the site. The fitting relation of all field stations (a), and part of sites which area are less than 10000 m^2; R^2 and P values are 0.34 and 0.06 (a), 0.46 and 0.06 (b), respectively. The blue area represents the 95% confidence interval and red lines represent fitting line.

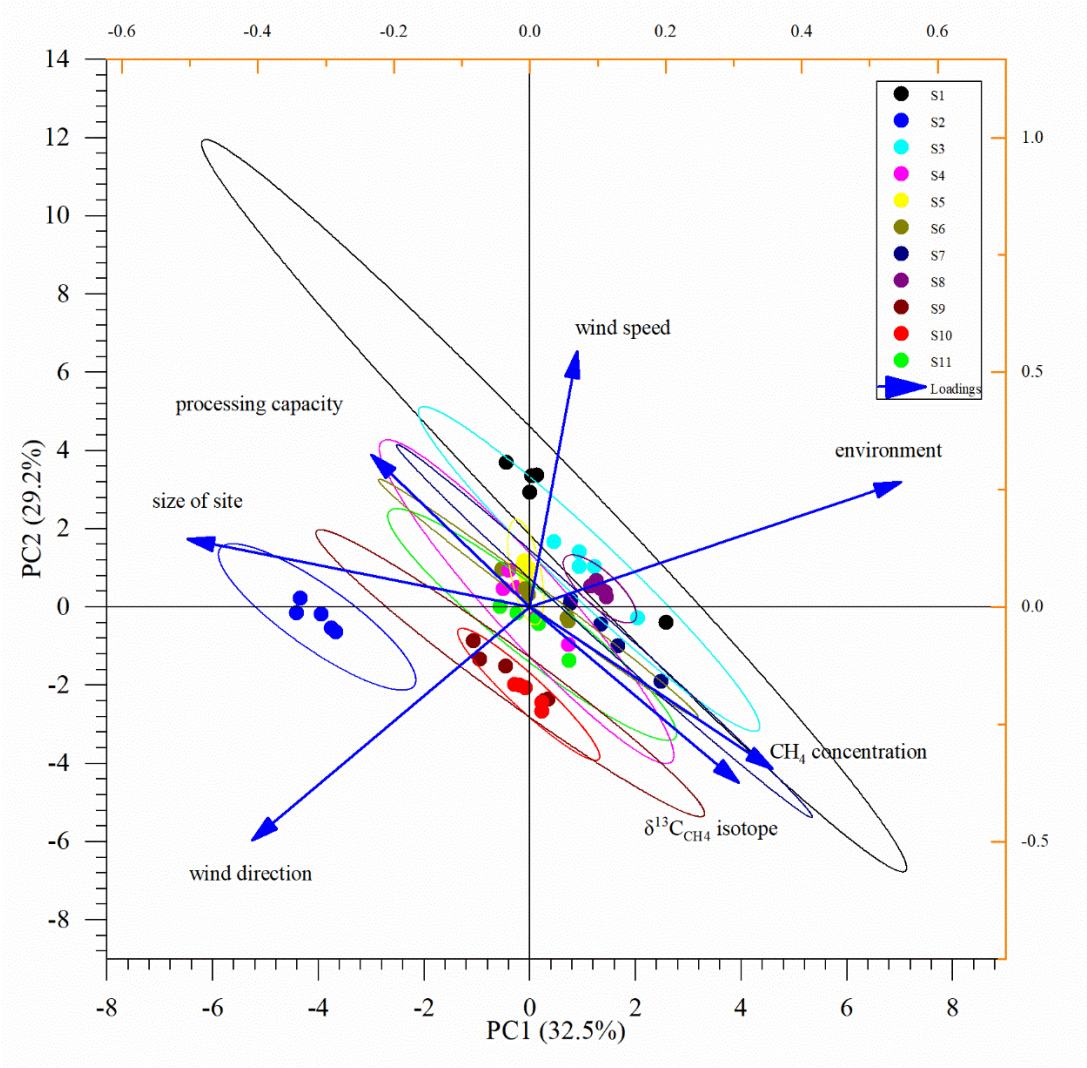

Fig. S7 Principal Component Analysis (PCA) of influencing factors of CH_4 isotope ($\delta^{13}C$) and mixing ratio in the field station. Including wind speed and direction, surrounding environment, size of the site and processing capacity.

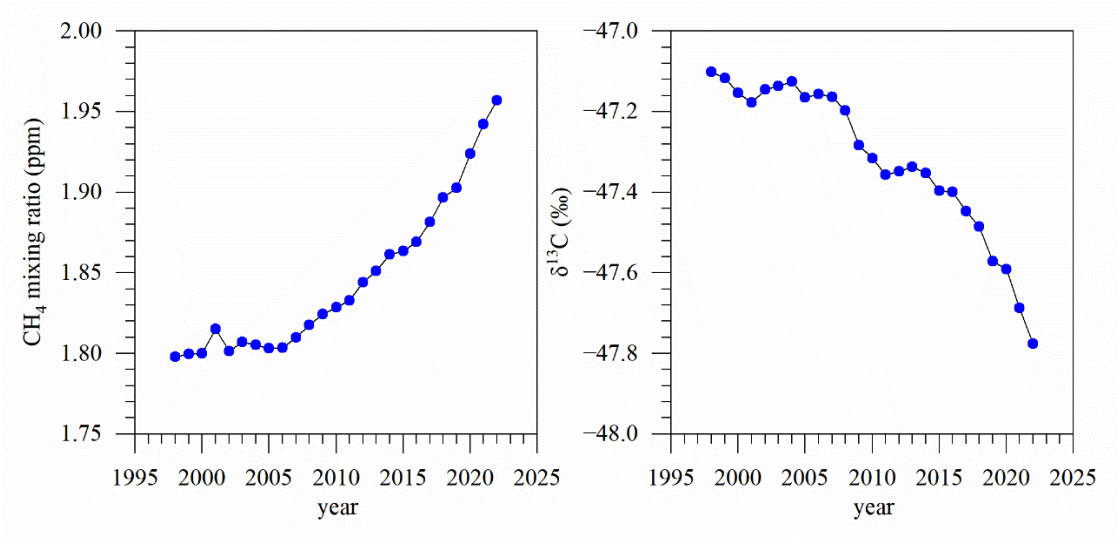

Fig. S8 Global average CH_4 mixing ratios (left) and $\delta^{13}C$ (right) from 1998 to 2022. The annual average values are available from the monthly mean data of the global observation sites, CH_4 mixing ratios data from 35 sites and $\delta^{13}C$ data from 20 sites.

References

1 Schwietzke, S. *et al.* Upward revision of global fossil fuel methane emissions based on isotope database. *Nature* **538**, 88-91 (2016).

2 Saunois, M. *et al.* Global Methane Budget 2000-2020. *Earth Syst. Sci. Data Discuss.* **2024**, 1-147 (2024). https://doi.org:10.5194/essd-2024-115

3 IEA. *Global Methane Tracker 2024*, <https://www.iea.org/reports/global-methane-tracker-2024> (2024).

4 Liu, Q. *et al.* Carbon and hydrogen isotopes of methane, ethane, and propane: A review of genetic identification of natural gas. *Earth-Science Reviews* **190**, 247-272 (2019).

5 Huang, S. *et al.* Multiple origins of the Paleogene natural gases and effects of secondary alteration in Liaohe Basin, northeast China: Insights from the molecular and stable isotopic compositions. *International Journal of Coal Geology* **172**, 134-148 (2017).

6 Wang, X. *et al.* Hydrogen isotope characteristics of thermogenic methane in Chinese sedimentary basins. *Organic Geochemistry* **83-84**, 178-189 (2015).

7 Yang, C. *et al.* Geochemical characteristics of pyrolysis gas from epimetamorphic rocks in the northern basement of Songliao Basin, Northeast China. *Science in China Series D: Earth Sciences* **51**, 140-147 (2008).

8 Cai, C., Zhang, C., He, H. & Tang, Y. Carbon isotope fractionation during methane-dominated TSR in East Sichuan Basin gasfields, China: A review. *Marine and Petroleum Geology* **48**, 100-110 (2013).

9 Cai, C. *et al.* Methane-dominated thermochemical sulphate reduction in the Triassic Feixianguan Formation East Sichuan Basin, China: towards prediction of fatal H2S concentrations. *Marine and Petroleum Geology* **21**, 1265-1279 (2004).

10 Hao, F. *et al.* Evidence for multiple stages of oil cracking and thermochemical sulfate reduction in the Puguang gas field, Sichuan Basin, China. *AAPG bulletin* **92**, 611-637 (2008).

11 Zhu, G., Wang, Z., Dai, J. & Su, J. Natural gas constituent and carbon isotopic composition in petroliferous basins, China. *Journal of Asian Earth Sciences* **80**, 1-17 (2014).

12 Wang, Y. *et al.* Origin of deep sour natural gas in the Ordovician carbonate reservoir of the Tazhong Uplift, Tarim Basin, northwest China: Insights from gas geochemistry and formation water. *Marine and Petroleum Geology* **91**, 532-549 (2018).

13 Zhang, S. *et al.* Unique chemical and isotopic characteristics and origins of natural gases in the Paleozoic marine formations in the Sichuan Basin, SW China: Isotope fractionation of deep and high mature carbonate reservoir gases. *Marine and Petroleum Geology* **89**, 68-82 (2018).